Investigating the production of liquid fuels from synthesis gas (CO + H$_2$) in a bench-scale packed-bed reactor based on Fe–Cu–La/SiO$_2$ catalyst: experimental and CFD modeling

Mohammad Irani

Abstract A computational fluid dynamic (CFD) and experimental study of Fischer–Tropsch Synthesis (FTS) process in a fixed-bed reactor is presented. The reactor was a 1.2 cm diameter and 80 cm length steel tube in which ceramic particles were employed to dilute the catalyst bed and thus prevent the emergence of hot spot in it. An axi-symmetric CFD model with an optimized mesh of 22,016 square cells was developed to model hydrodynamics, chemical reaction, and heat and mass transfer in the reactor. Thermodynamic non-ideal behavior of the gas mixture was modeled using Peng–Robinson equation of state. Kinetic models for FTS and water–gas-shift reaction rates based on Langmuir–Hinshelwood type for each of the species were employed. Good agreement was achieved between the bench experimental data and the model. Performing reactions inside packed-bed reactor due to high pressure and temperature is very difficult and expensive, and CFD simulations are considered as numerical experiments in many cases. A sensitivity analysis was run to find the effect of temperature, pressure, GHSV and H$_2$/CO ratio on the reactor performance. It was concluded that the obtained results from CFD analysis give precise guidelines for further studies on optimization of FTS fixed-bed reactor performance.

Keywords Fischer–Tropsch synthesis · GTL · Fixed-bed reactor · Fe–Cu–La/SiO$_2$ catalyst · CFD

List of symbols

P	Pressure (bar)
g	Gravity acceleration (m s^{-2})
v	Velocity (m s^{-1})
H	Total enthalpy (kJ kg^{-1} s^{-1})
h	Enthalpy of species (kJ kg^{-1} s^{-1})
j	Mass flux (kg m^{-2} s^{-1})
q	Heat flux (kJ m^{-2} s^{-1})
S	Momentum source term
D_{ij}	Diffusivity coefficient
C_i	Concentration (kmol m^3)
Z	Compressibility factor
T	Temperature (K)
f	Fugacity (bar)
k_i	Kinetic constant (mol h^{-1} g^{-1} bar^{-1})
E_i	Activation energy (kJ kmol^{-1})
R	Global gas factor (kJ kmol^{-1} K^{-1})
M_i	Molecular weight (kg kmol^{-1})
V	Volume (m^3)
x_i	Mass fraction
D	Total diffusivity coefficient (m^2 s^{-1})
k_m	Thermal conductivity (kJ m^{-1} K^{-1})

Greek letters

ρ	Density (kg m^{-3})
μ	Viscosity (kg m^{-1} s^{-1})
φ_i	Fugacity coefficient

Subscript

i	Species number
j	Second species number
m	Mixture

M. Irani (✉)
Gas Division, Research Institute of Petroleum Industry (RIPI),
West Blvd., Near Azadi Sports Complex, Tehran, Iran
e-mail: iranim@ripi.ir; mohammadirani@yahoo.com

Introduction

Gas to liquid (GTL) process refers to the technologies designed to convert natural gas and coal into liquid

hydrocarbons such as gasoline or diesel fuel. The Fischer–Tropsch technique consists of four major steps: (1) treatment of natural gas to remove water and impurities, (2) reforming of the natural gas to produce a mixture of carbon monoxide and hydrogen, called syngas, (3) Fischer–Tropsch synthesis (FTS) that produces heavier hydrocarbons from syngas and (4) upgrading to produce finished products. The reduction in exploitation rate of crude oil from reservoirs and discovery of new gas reserves in the world have made FTS more appealing in recent years. Also, some of the gas reservoirs are located in remote areas, and the transport of natural gas in these cases can be uneconomical. FTS can be used to convert natural gas into liquid fuels, and in this way the transport of energy source is much easier and economical [1].

Numerous researches have been made to understand, model and optimize this process. Some studies focused on the preparation, promotion and characterization of the catalysts [2–6] and kinetics of the FTS reactions [7–9], while some others worked on the effects of the operating conditions and combination of Fischer–Tropsch synthesis reactors on the performance of the reactor [10, 11].

Nakhaei Pour et al. [12] conducted several experiments and developed a set of production rates for FTS products.

Nowadays, thanks to the high speed of computational calculations, computational fluid dynamics (CFD) techniques have become a useful tool for understanding complex process phenomena [18–21].

Computational fluid dynamic simulations mean nothing, of course, independent of the reality they are supposed to represent. The accuracy of the simulation must be checked or validated against data obtained from real operating systems. This experimental validation is critical to ensure that the computational tools are meaningful representations of the applications for which they are intended. By predicting a system's performance in various areas, CFD can potentially be used to improve the efficiency of existing operating systems as well as the design of new systems. It can help to shorten product and process development cycles, optimize processes to improve energy efficiency and environmental performance, and solve problems as they arise in plant operations. Since doing reaction experiments inside packed-bed reactor is very difficult and expensive, CFD simulations are considered as numerical experiments.

CFD has also been applied to determine optimum control strategies and optimize equipment in chemical industries and has been especially successful in the aerospace industry. Troshko and Zdravistch [22] developed a CFD model for FTS bubble column reactors. Their object was quantitative prediction of reactor performance for design purposes. In their model, chemical reactions, gas bubble size and the effects of the catalyst present in the liquid phase were considered. They validated their model by comparing the results with experimental data and published data from modeling of an industrial reactor. Although heat transfer effect had not been considered, it was concluded from analysis of FT rate that to control the reactor temperature, appropriate heat removal devices are required next to the gas injection region when the syngas flow rate is low. Arzamendi et al. [23] employed ANSYS CFX software to develop a three-dimensional CFD model for heat transfer in an FTS microchannel reactor. The effects of feed and cooling water flow rates and pressure on the performance of the reactor were discussed. It was concluded that buoyancy forces have significant effects on heat performance of the micro reactor. A kinetic model was formulated and implemented the rate equations in CFD codes. Fixed-bed reactors are commonly used in FTS [24]. Research is ongoing to convert natural gas into liquid fuel in an optimized and effective way [13, 14]. Therefore, executable cases should be modeled and optimized to attain this goal [15–17].

Iran's proved natural gas reserves are about $1,045.7 \times 10^{12}$ cu ft. (29,610 km^3) or about 15.8 % of the world's total reserves, of which 33 % are in associated gas and 67 % in non-associated gas fields. It has the world's second largest reserves after Russia [13]. This huge amount of gases can be converted to synthesis fuels. The Research Institute of Petroleum Industry, National Iranian Oil Company (RIPI-NIOC) carried out a wide range of experimental and modeling investigations in this area. In our previous work, FTS fixed-bed reactor based on iron–zeolite catalyst was studied. Saturated water was utilized as a scraper of reaction heat and it was concluded that the temperature run away was controlled using saturated water; so that the maximum temperature rise within the catalyst bed was 16 K [25]. In the present work, a CFD model was developed to model FTS in a fixed-bed Fe–Cu–La/SiO$_2$ catalyst reactor. The experiments were conducted in a bench-scale reactor. To avoid the hot spots, the catalytic bed was diluted with ceramic beads. Adequate equation of state was employed to model the non-ideality of the gas mixture [26, 27]. The model predictions were validated with bench experimental data.

Materials and methods

Process description

The used reactor and a schematic description are shown in Fig. 1 and its characteristics are given in Table 1. It was designed and constructed by the Research Institute of Petroleum Industry, National Iranian Oil Company (RIPI-NIOC) in 2009 [12]. The reactor was packed with Fe–SiO$_2$
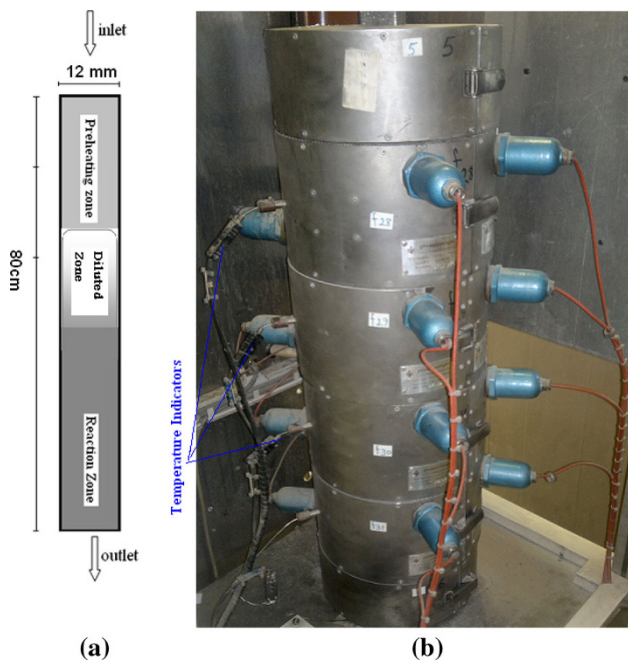
Fig. 1 FTS fixed-bed reactor. **a** Real photograph, **b** schematic view

Table 1 FTS pilot plant characteristics

Tube dimension (mm)	$12 \times 1 \times 800$
Number of tubes	1
Molar ratio of H_2/Co	1
Feed temperature (K)	563, 573 and 583
Catalyst sizes (mm)	0.5×1
Catalyst density (kg/m^3)	1,290
Bulk density (kg/m^3)	730
Reactor pressure (bar)	17
GHSV (nl/h)	3
Bed voidage	0.28

catalyst (with atomic ratios as: 100 Fe/5.64 Cu/2 La/ 19 Si). There was a heater jacket around the reactor through which heat supply for the required reaction temperature was provided. To prevent the creation of hot spot at the beginning of the catalyst bed, (location of the gas entering the bed) it was diluted using ceramic particles. The experiments were carried out at different operating conditions and the temperature profile along the reactor and the product composition were analyzed.

CFD modeling

Solution strategy and boundary conditions

A 1.2 cm $\times$ 80 cm axi-symmetric model consisting of one entrance preheating fluid zone and a packed reaction zone was utilized to model the reactor. A uniform structured grid with 22,016 meshes was employed and the model predictions were checked to be independent of the mesh size. The packed bed was considered as a porous medium due to the large value of N (tube-to-catalyst diameter ratio) [28]. A zone was considered as diluted reaction zone between preheated and reaction zones. In this region, the reaction rate was multiplied by catalyst to mixture (catalyst + ceramic) mass ratio and consequently the resulting rate was lesser than before. The unit of the published chemical rate expressions is kg mol/(kg cat s). It can be multiplied by catalyst/mixture ratio, F_{cat}, to give the real reaction rate (s_i) that is implemented in the CFD code:

$$S_i = r_i \times F_{cat}[=] \frac{\text{kg mol}}{\text{kg cat s}} \times \frac{\text{kg cat}}{(\text{kg cat} + \text{kg ceramic})}$$
$$= \frac{\text{kg mol}}{(\text{kg cat} + \text{kg ceramic})\ \text{s}}. \tag{1}$$

Mass-flow-inlet and pressure-outlet boundary conditions were used for reactor inlet and outlet, respectively. Constant temperature and no-slip condition was employed for the reactor walls. The finite volume method was used to discretize the partial differential equations of the model. The SIMPLE algorithm was employed for pressure–velocity coupling. The solution procedure is described in Fig. 2. The convergence criterion was based on the residual value of the calculated variables, namely mass, velocity components, and energy and species mass fractions. In the present calculations, the numerical computation was considered to be converged when the scaled residuals of the different variables were lower than 10^{-4} for continuity and momentum equations and 10^{-7} for the other variables.

Conservation equations

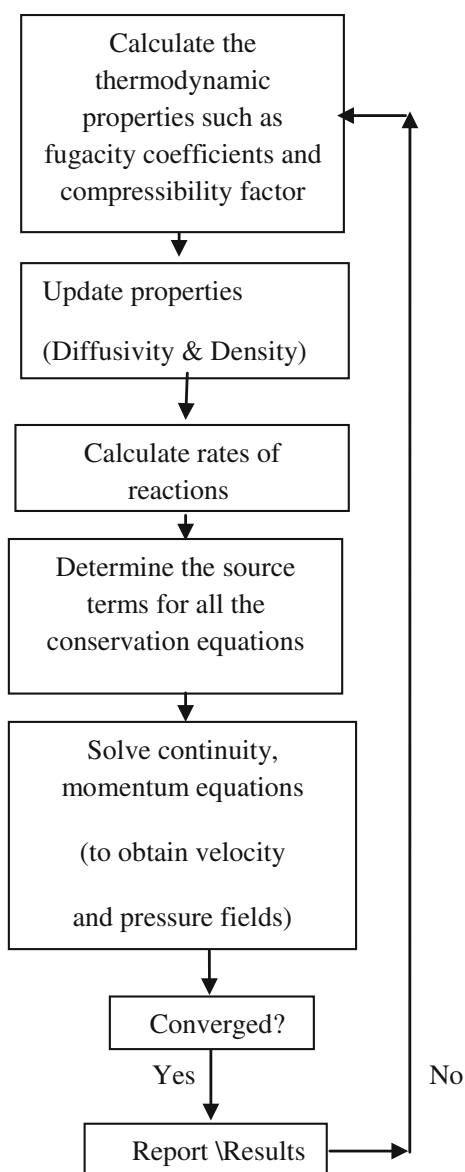The mass conservation, momentum, energy and species can be expressed as:

Mass: $\nabla \cdot (\vec{v}\rho) = 0$ $\qquad\qquad$ (2)

Momentum: $\nabla \cdot (\rho\vec{v}\vec{v}) = -\nabla P + \nabla \cdot \left[\mu(\nabla\vec{v} + \nabla\vec{v}^T)\right]$
$$+ \rho g + S \tag{3}$$

Energy: $\nabla \cdot (\vec{v}(\rho H + P)) + \nabla \cdot \left(\sum_{i=1}^{n} h_i j_i\right)$
$$= -\nabla \cdot (q) + S_R \tag{4}$$

Species: $\nabla \cdot (\vec{v}C_i - D_i\nabla C_i) = R_i,$ $\qquad$ (5)

where ρ represents the mixture density, $\vec{v}$ is the velocity vector, and H and h_i are the total enthalpy and enthalpy of the species, respectively. P is the static pressure and C_i

Fig. 2 The solution procedure

stands for the concentration of the chemical species. The catalyst region was considered as a porous medium and modeled by the addition of a momentum source term:

$$S = -\left(\sum_{j=1}^{2} D_{ij} \mu v_j + \sum_{j=1}^{2} C_{ij} \frac{1}{2} \rho |v| v_j \right). \tag{6}$$

The momentum source term is composed of two parts: a viscous loss term (Darcy, the first term on the right-hand side of Eq. 6) and an inertial loss term (the second term on the right-hand side of Eq. 6). $|v|$ is the magnitude of the velocity and D and C are prescribed matrices. In this work, the flow in the reactor is laminar; therefore, the inertial term was ignored [29]. S_R in Eq. (4) is the source of energy caused by the chemical reaction:

$$S_R = -\left(\sum_j \frac{h_j^0}{M_j} R_j \right). \tag{7}$$

The temperature constant was defined at the walls to establish an isothermal condition at the wall boundaries.

Physical properties

The non-ideal thermodynamic behavior of the system due to the presence of heavy products and the operating conditions [26, 27] was predicted using Peng–Robinson equation of state:

$$\ln \widehat{\varphi}_i = (Z - 1)\frac{b_i}{b_m} - \ln(Z - \beta) - I\bar{q}_i, \quad q = \frac{a}{bRT},$$

$$\bar{q}_i = q\left(2 \times \frac{\frac{\partial a}{\partial X_i}}{a} - \frac{b_i[i]}{b} \right)$$

$$I = \frac{1}{\varepsilon_1 - \varepsilon_2} \ln\left(\frac{Z + \varepsilon_1 \times \beta}{Z + \varepsilon_2 \times \beta} \right), \quad beta = \frac{bP}{RT}, \quad f_i = \widehat{\varphi}_i \times P \times y_i, \tag{8}$$

where f_i is species fugacity, R is the universal gas constant, MG is the molecular weight of gas mixture and P is the operating pressure (taken to be 17 bar). Z is the compressibility factor for calculation of the mixture density:

$$\rho = \frac{PM}{ZRT} \tag{9}$$

The parameters of Eq. (8) are listed in Table 2. The specific heat of each species was defined as piecewise-polynomial function of temperature. Other thermal properties of the mixture such as molecular viscosity, thermal conductivity and diffusivity coefficient were calculated from Poling et al. [30].

Reaction rate expressions

Twenty-five chemical species including CO, H_2, CO_2, H_2O and C_1–C_{21}, were considered as reactants and products of the FTS reactions. The leading Fischer–Tropsch chemical reactions are listed in Table 3.

The general form of rate equations for production of C_i is expressed as [12]:

$$R_{C_i} = \frac{0.011 f_{H_2}^{0.7} f_{CO}^{-0.9}}{\left(2.2 - 0.18 \frac{f_{H_2}}{f_{CO}} \right)^{i-1}} \qquad i = 4 - 9 \tag{10}$$

$$R_{C_i} = \frac{3 \times 10^{-5} f_{H_2}^{1.7} f_{CO}^{-1.1}}{\left(1.14 - 0.069 \frac{f_{H_2}}{f_{CO}} \right)^{i-1}} \qquad i = 11 - 22 \tag{11}$$

$$R_{C_1} = 0.001518 * f_{H_2}^{0.241} / f_{CO}^{0.241} \tag{12}$$

Table 2 Parameters of Peng–Robinson EOS

σ	ε	Ω	Ψ
$1 + \sqrt{2}$	$1 - \sqrt{2}$	0.07779	0.45724

$$\alpha(T_r; \omega) = \left[1 + (0.37464 + 1.54226\omega - 0.26992\omega^2)(1 - T_r^{1/2}) \right]^2$$

$$Z = \beta + (Z + \varepsilon\beta)(Z + \sigma\beta)\left(\frac{1 + \beta - Z}{q\beta}\right), \beta = \Omega\frac{P_r}{T_r}, q = \frac{\alpha(T_r)\psi}{\Omega T_r}$$

Table 3 List of FTS reactions

Number	Reaction stoichiometry
1	$nCO + (n+1)H_2 \rightarrow C_nH_{2n+2} + nH_2O$
2	$CO + H_2O \rightarrow CO_2 + H_2$

$$R_{C_2} = 0.01819 * f_{H_2}^{0.045}/f_{CO}^{0.045} \tag{13}$$

$$R_{C_3} = 0.011 * f_{H_2}^{0.7}/f_{CO}^{0.9} \tag{14}$$

$$R_{C_{10}} = 3 \times 10^{-5} * f_{H_2}^{1.7}/f_{CO}^{1.1}. \tag{15}$$

Reaction (2) is known as water–gas-shift (WGS) reaction and its rate can be expressed as [31]:

$$R_{WGS} = \frac{k_w(f_{CO}f_{H_2O} - f_{CO_2}f_{H_2}/K_{WGS})}{(1 + K_1f_{CO} + K_2f_{H_2O})^2}.$$

The kinetic parameters of WGS reaction rate are given in Table 4 where K_{WGS} is the equilibrium constant and can be calculated as follows:

$$\log K_{WGS} = \left(\frac{2,073}{T} - 2.029\right). \tag{16}$$

Results and discussion

The gas mixture compressibility factor along the reactor is shown in Fig. 3. The figure shows that due to formation of widespread range of hydrocarbon (C₁–C₂₁) and H₂O, the behavior of the system is non-ideal, so that Z descends below 0.9; thus, employing an equation of state for the estimation of physical and thermodynamic properties is necessary. The predicted values of C₅₊ selectivity and CO mole percent in the reactor outlet and temperature at three points along the reactor (point 1: beginning of catalytic bed; point 2: middle of catalytic bed; point 3: end of catalytic bed) were compared with experimental measurements and the simulation results are given in Table 5.

The operating condition for this comparison is completely similar for the experiment and simulation ($T = 573,563$; $P = 17$ bar; GHSV = 2,000; H₂/CO = 1). The values in this table show that the error values are less than 3 % for all of the compared variables. Considering the

Table 4 Rates parameters for WGS reaction

Parameter	Value
k_w	0.25 mmol g cat⁻¹ S⁻¹ bar⁻²
K_1	0.39 bar⁻¹
K_2	3.54 bar⁻¹
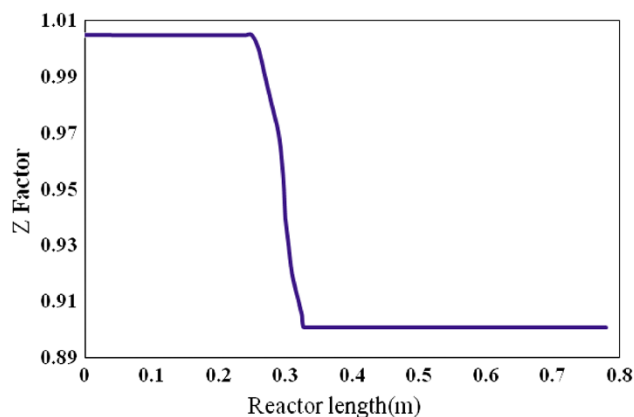
Fig. 3 Gas mixture compressibility factor along the reactor

aforementioned results, the model in this work can successfully predict the performance of the fixed-bed FT process.

The contour plots of temperature inside the reactor are presented in Fig. 4. The figure shows that the inside temperature of the reactor was controlled at the desired inlet temperature using ceramic particles in front of the catalyst bed. The particles acts as inert and reduce the rate of reaction which results in less heat of reaction and lower temperature rise. The reactants have maximum concentration at the beginning of the catalytic bed, so the highest rate of reaction occurs in this location. There is a temperature raise of about 16 K at the beginning of the reaction zone, due to the high concentration of the reactants and the consequent high rate of exothermic reactions in this region. Figure 5 shows the species mass fraction profiles along the reactor for the case with inlet gas temperature of 573 K. Due to the consumption of reactants, their concentrations are reduced along the reactor. Thus, the reaction rates are reduced and consequently the slopes of concentration curves along the reactor are decreased. The figure interprets that the main changes in the concentrations of reactants and products occur in the beginning of the reaction zone except for CO and ethane. Ethene acts as a monomer or building block during the FTS. Readsorption of ethene will result in a decrease of the ethane yield and an increase of higher hydrocarbons [32, 33]. This effect was included in the ethane production rate (the power of CO and H₂ concentration in Eq. (12) is much less than that in other rate

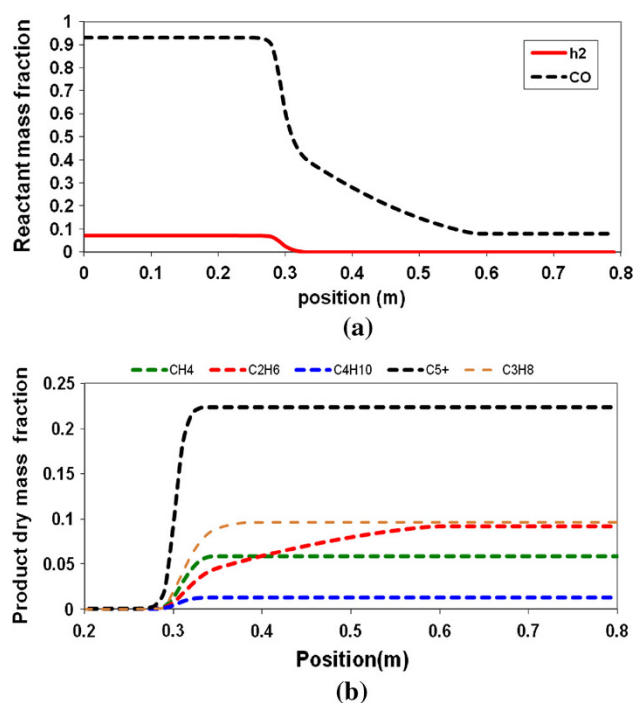**Table 5** Comparison between measured and predicted values for the bench-scale FTS processes

		Experimental	Simulation	|%Error|
GHSV = 2,000	CO conversion (%)	72.25	74.05	2.5
T = 573	C_{5+} selectivity	32.4	31.7	2.1
H_2/CO = 1	Temperature at point 1 (K)	575	589	2.4
P = 17 bar	Temperature at point 2 (K)	575	573	0.3
	Temperature at point 3 (K)	573	573	0
GHSV = 2,000	CO conversion (%)	67.53	65.05	2.5
T = 563	C_{5+} selectivity	34.8	32.7	2.1
H_2/CO = 1	Temperature at point 1 (K)	573	589	2.4
P = 17 bar	Temperature at point 2 (K)	575	573	0.3
	Temperature at point 3 (K)	573	573	0
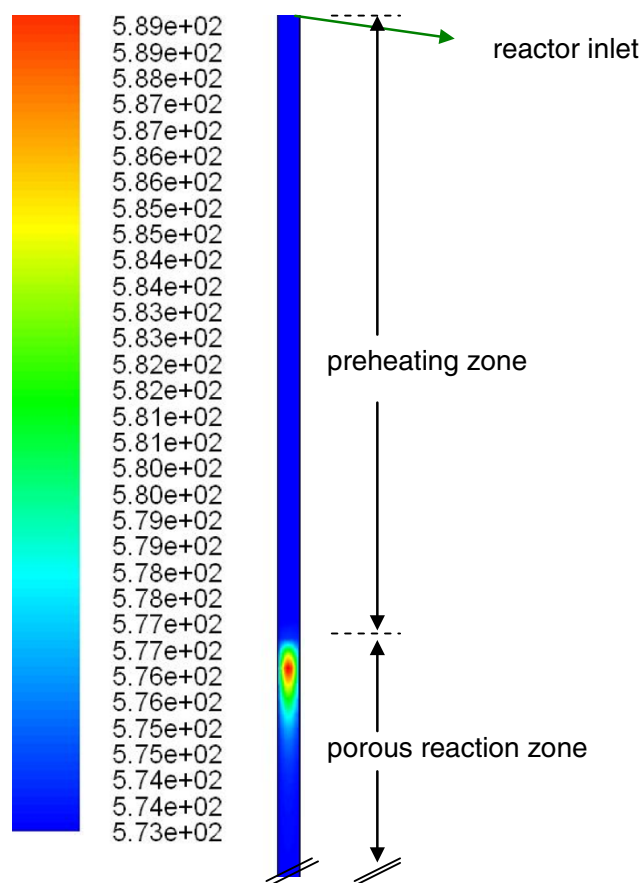
Fig. 4 Contour of temperature (operating condition: T = 573, P = 17 bar)

**Fig. 5** Mass fraction of species along the reactor length at T = 573

equations). The difference between concentration profile of CO and the other species can also be related to this matter.

Figure 6 shows that the mixture density increases along the reactor length due to the production of heavier hydrocarbons. Figure 7 presents the contours of velocity in the reactor. As can be seen, the radial velocity distribution and zero velocity near the walls due to the non-slip wall boundary condition are well predicted, as is naturally expected. Pressure drop in the porous region causes the gas

velocity to become almost uniform in the radial direction. In addition, because of the production of heavy products, the velocity magnitude significantly reduces by entering the reaction region. As mentioned before, the errors between experiment and simulation are below 3 % and the validated model can be used for further study. To investigate the effects of temperature, GHSV, pressure and H_2/CO ratio on the reactor performance, the reactor model was run at four different levels for each of the operating parameters. In all cases, one parameter was varied and the other parameters were kept constant. The C_{5+} selectivities (g C_{5+}/g converted feed) for different temperatures are shown in Fig. 8.
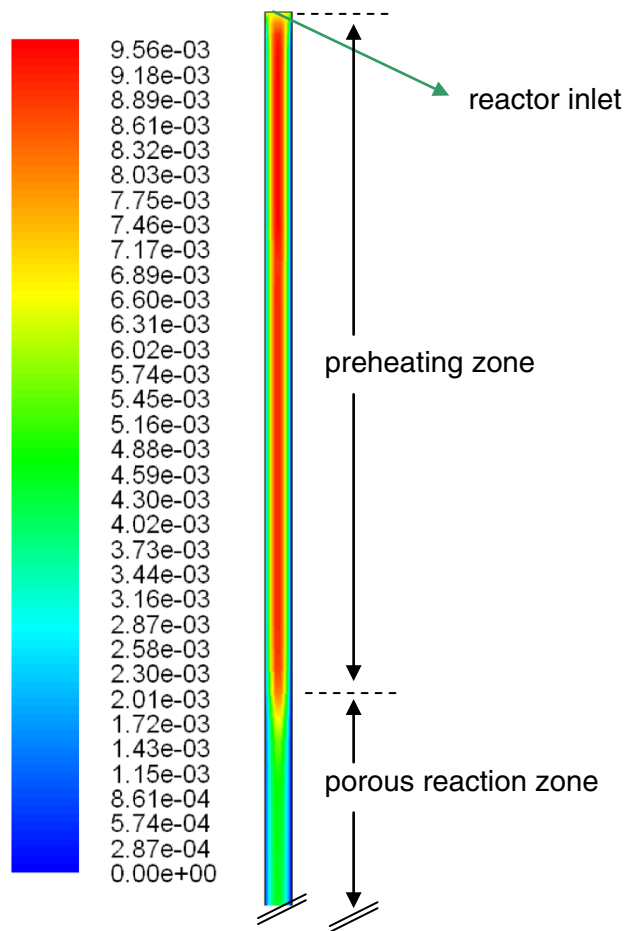
As depicted in this figure, increasing the temperature from 543 to 553 K increases the C_{5+} selectivity. However, further increasing the temperature to 563 K decreases C_{5+} selectivity.
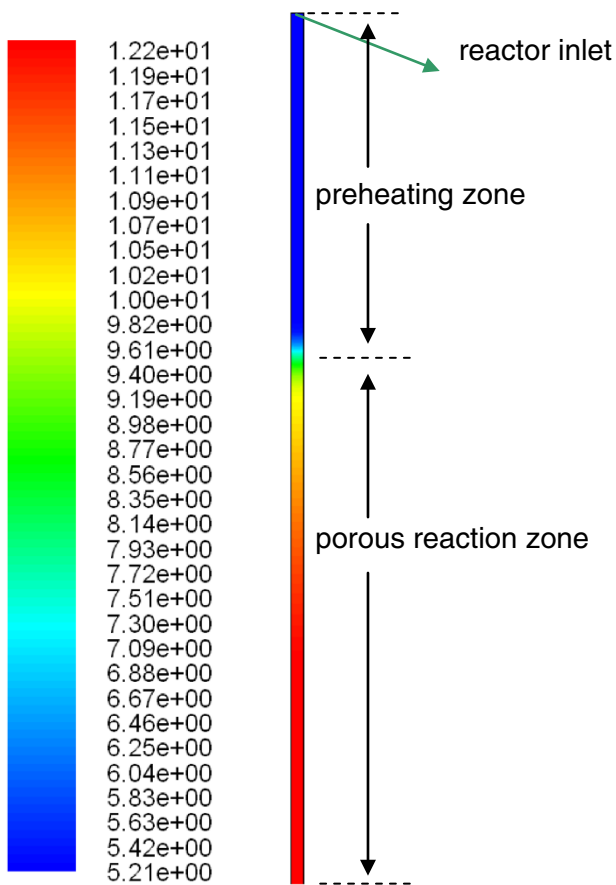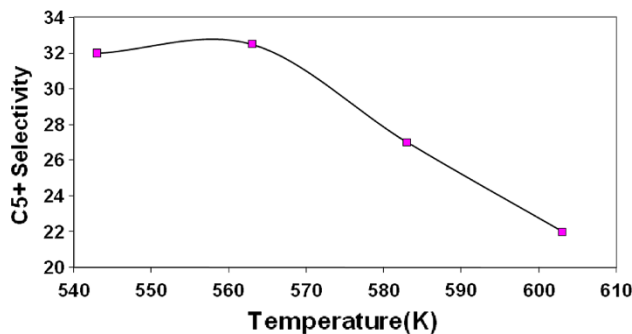
Fig. 6 Contour of density (operating condition: $T = 573$, $P = 17$ bar)

Fig. 7 Contour of velocity (operating condition: $T = 573$, $P = 17$ bar)

It should be noted that increasing the reactor temperature has, as a consequence, two opposite effects: firstly, it increases the rate of reactions; secondly, it shifts WGS reaction to reactants. In increasing the temperature from 553 to 563 K, the second effect is dominant and the production of C_{5+} decreases due to the reduction in the concentration of H_2.

Figure 9 shows that the decrease in GHSV causes a descending trend in the C_{5+} selectivity due to reduction in the residence time. The effects of H_2/CO molar ratio on C_{5+} selectivity are presented in Fig. 10. As the H_2/CO molar ratio increases, the amount of available H_2 for the reaction increases and the growth of polymerization chain is stopped by H_2 (H_2 participates in the termination step reactions) [34]. Consequently, the production rate of heavier hydrocarbons decreases. Pressure is the other parameter that affects the production of C_{5+}. With increasing total pressure, the reactant partial pressure is increased which results in increase of C_{5+} and water as products. The production of water more than the threshold value has a negative effect on C_{5+} selectivity. As seen in Fig. 11, the C_{5+} selectivity increases as the pressure increases from 13 to 21 bar and decreases with increase to 25 bar.
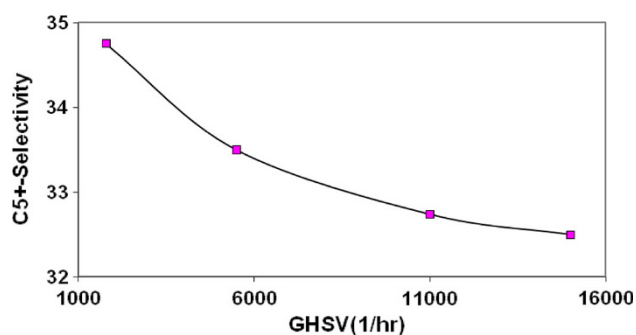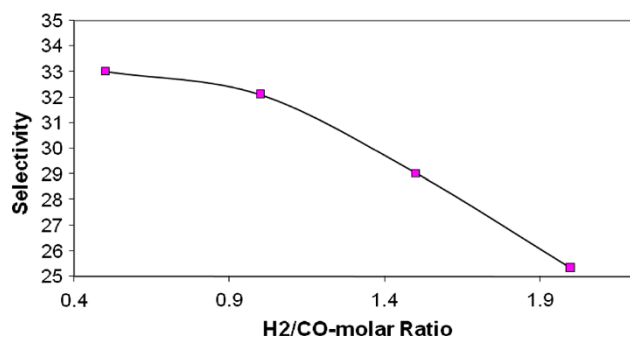

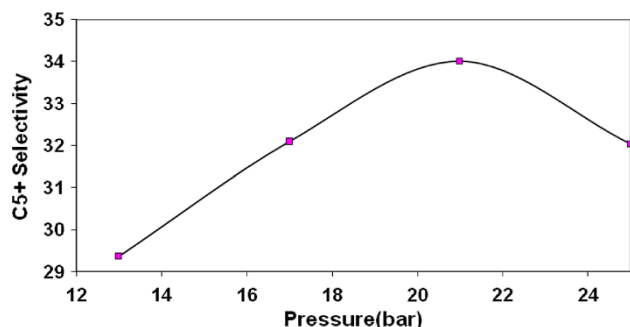**Fig. 8** Selectivity of C_{5+} at different temperatures: CFD prediction

Conclusions

A two-dimensional CFD model was developed to model fluid flow, chemical reaction, and heat and mass transfer in a fixed-bed reactor. The non-ideal thermodynamic behavior of the mixture was modeled using Peng–Robinson EOS. The temperature runaway of the process was quenched using dilution of catalyst bed with ceramic particles. The

Fig. 9 Selectivity of C_{5+} at different GHSVs: CFD prediction

Fig. 10 Selectivity of C_{5+} at different H_2/CO molar: CFD prediction

Fig. 11 Selectivity of C_{5+} at different pressures: CFD prediction

model was validated against the experimental data from a bench-scale FTS reactor in several aspects and good agreements were found. The validated model was used to study the effect of operating conditions such as system temperature and pressure, GHSV and H_2/CO molar ratio on reactor performance. The results showed that the aforementioned parameters have different effects on the C_{5+} selectivity and the trend of these effects studied and reported. Optimum values of these parameters can be found to reach the maximum yield. It was found that each of the parameters has an optimum for the examined operating

conditions of pressure, feed composition and flow rate. In this study the effect of a single parameter was evaluated and the other factors were considered fixed, while the interaction of these parameters may have different effects. Hence since the model has proven to be in good agreement with the experimental data, it could be used in further studies to find more accurate values for the optimum conditions of temperature and GHSV without the need for hard experimental studies.

References

1. Keshav TR, Basu S (2007) Gas-to-liquid technologies: India's perspective. Fuel Process Technol 88:493–500
2. Tavasoli A, Khodadadi A, Mortazavi Y, Sadaghiani K, Ahangari MG (2006) Lowering methane and raising distillates yields in Fischer–Tropsch synthesis by using promoted and unpromoted cobalt catalysts in a dual bed reactor. Fuel Process Technol 87:641–647
3. Tavasoli A, Trépanier M, Malek Abbaslou RM, Dalai AK, Abatzoglou N (2009) Fischer–Tropsch synthesis on mono- and bimetallic Co and Fe catalysts supported on carbon nanotubes. Fuel Process Technol 90:1486–1494
4. Tavasoli A, Nakhaeipour A, Sadaghiani K (2007) Raising Co/Al_2O_3 catalyst lifetime in Fischer–Tropsch synthesis by using a novel dual-bed reactor. Fuel Process Technol 88:461–469
5. Zhou W, Chen JG, Fang KG, Sun YH (2006) The deactivation of CO/SiO_2 catalyst for Fischer–Tropsch synthesis at different ratios of H_2 to CO. Fuel Process Technol 87:609–616
6. Mirzaei AA, Babaei AB, Galavy M, Youssefi A (2010) A silica supported Fe–Co bimetallic catalyst prepared by the sol/gel technique: operating conditions, catalytic properties and characterization. Fuel Process Technol 91:335–347
7. Sari A, Zamani Y, Taheri SA (2009) Intrinsic kinetics of Fischer–Tropsch reactions over an industrial Co–Ru/γ-Al_2O_3 catalyst in slurry phase reactor. Fuel Process Technol 90:1305–1313
8. Haghtalab A, Nabipoor M, Farzad S (2011) Kinetic modeling of the Fischer–Tropsch synthesis in a slurry phase bubble column reactor using Langmuir–Freundlich isotherm. Fuel Process Technol [corrected proof]
9. Schulz H, Beck K, Erich E (1988) Kinetics of Fischer–Tropsch selectivity. Fuel Process Technol 18:293–304
10. Woo KJ, Kang SH, Kim SM, Bae JW, Jun KW (2010) Performance of a slurry bubble column reactor for Fischer–Tropsch synthesis: determination of optimum condition. Fuel Process Technol 91:434–439
11. Calleja G, Lucas AD, Grieken RV (1995) Co/HZSM-5 catalyst for syngas conversion: influence of process variables. Fuel 74(3):445–451
12. Nakhaei Pour A, Housaindokht MR, Tayyari SF, Zarkesh J (2010) Effect of nano-particle size on product distribution and kinetic parameters of Fe/Cu/La catalyst in Fischer–Tropsch synthesis. J Nat Gas Chem 19:107–116
13. Rahimpour MR, Elekaei H (2009) A comparative study of combination of Fischer–Tropsch synthesis reactors with hydrogen-permselective membrane in GTL technology. Fuel Process Technol 90:747–761

14. Rahimpour MR, Forghani AA, Khosravanipour Mostafazadeh A, Shariati A (2010) A comparison of co-current and counter-current modes of operation for a novel hydrogen-permselective membrane dual-type FTS reactor in GTL technology. Fuel Process Technol 91:33–44

15. Liu QS, Zhang ZX, Zhou JL (1999) Steady state and dynamic behaviour of fixed bed catalytic reactor for Fischer–Tropsch synthesis. I. Mathematical model and numerical method. J Nat Gas Chem 8(2):137–180

16. Liu QS, Zhang ZX, Zhou JL (1999) Steady state and dynamic behaviour of fixed bed catalytic reactor for Fischer–Tropsch synthesis. II. Steady state and dynamic simulation results. J Nat Gas Chem 8(3):238–265

17. Wang Y, Xu Y, Li Y, Zhao Y, Zhang B (2003) Heterogeneous modeling for fixed-bed Fischer–Tropsch synthesis: reactor model and its applications. Chem Eng Sci 58(3–6):867–875

18. Shah KV, Vuthaluru R, Vuthaluru HB (2009) CFD based investigations into optimization of coal pulveriser performance: effect of classifier vane settings. Fuel Process Technol 90:1135–1141

19. Bhambare KS, Ma Z, Lu P (2010) CFD modeling of MPS coal mill with moisture evaporation. Fuel Process Technol 91:566–571

20. Vuthaluru R, Vuthaluru HB (2006) Modelling of a wall fired furnace for different operating conditions using FLUENT. Fuel Process Technol 87:633–639

21. Pallarés J, Gil A, Cortés C, Herce C (2009) Numerical study of co-firing coal and *Cynara cardunculus* in a 350 MWe utility boiler. Fuel Process Technol 87(90):1207–1213

22. Troshko AA, Zdravistch F (2009) CFD modeling of slurry bubble column reactors for Fisher–Tropsch synthesis. Chem Eng Sci 64(5):892–903

23. Arzamendi G, Diéguez PM, Montes M, Odriozola JA, Sousa-Aguiar EF, Gandía LM (2010) Computational fluid dynamics study of heat transfer in a microchannel reactor for low-temperature Fischer–Tropsch synthesis. Chem Eng J 160(3):915–922

24. Steynberg AP, Dry ME, Havis BH, Berman BB (2004) Chapter 2 Fischer–Tropsch reactors. Stud Surf Sci Catal 152:64

25. Irani M, Alizadehdakhel A, Nakhaeipour A, Prolx P, Tavassoli A (2011) An investigation on the performance of a FTS fixed-bed reactor using CFD methods. Int Commun Heat Mass Transfer 38:1119–1124

26. Irani M, Bozorgmehry RB, Pishvaie MR, Tavasoli A (2010) Investigating the effects of mass transfer and mixture non-ideality on multiphase flow hydrodynamics using CFD methods. Iran J Chem Chem Eng 29(1):51–60

27. Irani M, Bouzarjomehri RB, Pishvaei MR (2010) Impact of thermodynamic non-idealities and mass transfer on multi-phase hydrodynamics. Scientia Iranica 17(1):55–64

28. Foumeny EA, Moallemi HA, Mcgreavy C, Castro JAA (1991) Elucidation of mean voidage in packed beds. Can J Chem Eng 69(4):1010–1015

29. Fluent, Incorporated (2001) FLUENT 6 USER Manual. Fluent Inc., Lebanon

30. Poling BE, Prausnitz JM, O'Connell JP (2000) The properties of gases and liquids, 5th edn. McGraw-Hill, New York

31. Nakhaei Pour A, Housaindokht MR, Tayyari SF, Zarkesh J, Kamali Shahri SM (2011) Water–gas-shift kinetics over a Fe/Cu/La/Si catalyst in Fischer–Tropsch synthesis. Chem Eng Res Des 9:262–326

32. Sarup B, Wojciechowski BW (1988) Studies of the Fischer–Tropsch synthesis on a cobalt catalyst i. evaluation of product distribution parameters from experimental data. Can J Chem Eng 66:831

33. Novak S, Madon RJ, Suhl H (1982) Secondary effects in the Fischer–Tropsch synthesis. J Catal 77:141

34. van der Laan GP, Beenackers AACM (1999) Kinetics and Selectivity of the Fischer–Tropsch Synthesis: a literature review, catalysis reviews. Catal Rev Sci Eng 41(3&4):255–318